Mechanisms of thermal equilibration in doped amorphous silicon

R. A. Street, M. Hack, and W. B. Jackson
Xerox Corporation, Palo Alto Research Center, Palo Alto, California 94304
(Received 3 August 1987)

Experimental and theoretical investigations of the mechanisms of thermal equilibration in *n*-type amorphous silicon are presented. The time, temperature, and doping dependence of the band-tail electron density is obtained from sweep-out experiments, and the dangling-bond and donor densities from photothermal deflection spectroscopy (PDS), bias annealing, and *C-V* characteristic measurements. An important new result is that donors participate in the equilibration, and that the doping efficiency can be greatly enhanced by a depletion bias. Numerical modeling of the transport allows us to deduce the changes in the density of states and in the position of the Fermi energy, both in equilibrium and in the frozen-in state. The equilibrium state is derived by minimizing the free energy of the doped *a*-Si:H using a simple density-of-states model. With this approach, the electronic properties (doping efficiency, conductivity, Fermi energy, etc.) can be computed and are shown to be in fairly good agreement with all the experimental results, although the observed lack of temperature dependence of the dangling-bond density remains a puzzle. Further evidence is presented that hydrogen motion is the underlying mechanism of equilibration, and we develop a qualitative model to describe the bonding and movement of hydrogen, based on a distribution of weak Si—Si bonds.

I. INTRODUCTION

Recent experiments have found that some electronic properties of hydrogenated amorphous silicon (*a*-Si:H) can be described by a glasslike thermal equilibrium.[1–4] This means that equilibrium is rapidly established near the deposition temperature, but as the material is cooled, the structural changes needed to maintain equilibrium become increasingly slow, and eventually the structure freezes into a nonequilibrium state. The properties below the equilibration temperature are therefore determined by the kinetics of cooling as in a conventional glass. This type of behavior has now been observed, mostly from electronic transport measurements, in both doped and undoped *a*-Si:H. The equilibration temperature is in the range 100–200 °C for slow cooling rates, and is lowest in *p*-type material and highest in undoped material.

There are two characteristic aspects to the equilibration process which need further explanation. One is the nature of the equilibrium state, which is described by the thermodynamically stable state (lowest free energy) from amongst the set of accessible configurations. The second aspect is the kinetics by which the system approaches equilibrium, which is particularly important at low temperatures when the equilibration time becomes sufficiently long to freeze in a nonequilibrium state. The detailed mechanisms of these two processes, particularly in *n*-type doped material, is the subject of this paper.

In order to understand the equilibrium from a thermodynamic point of view, information is needed about the set of structural configurations that participate, and their formation energies. This has led us to study the temperature-dependent changes in the density of states and in the electron or hole distributions.[1,2,5] The transport measurements from which the equilibration has been observed are controlled by the localized state distribution. Thus most models focus on band-tail states, donor and acceptor impurity states, and deep defects.[2,6–9] In our previous studies the equilibrium was observed by sweep-out and conductivity data, both of which depend particularly on the density and distribution of defect and dopant states.[1,2] We developed a model based on the defect compensation description of doping,[10] in which the principal variables are the densities of the different types of states. On the other hand, Bar-Yam *et al.*[8] have proposed a theory in which the *shape* of the gap state distribution as well as the density is modified by the thermal equilibrium, and Smith and Wagner[9] have related the equilibrium in undoped *a*-Si:H to the distribution of the valence-band tail.

Concerning the kinetics of equilibration, we have proposed that the origin is the motion of bonded hydrogen, with the silicon matrix being essentially rigid.[1,11] Measurements of hydrogen diffusion find that the rate of hydrogen motion can quantitatively account for the equilibration data.[1,12] However, other groups have suggested that structural rearrangements not involving hydrogen may be important.[8] Here we discuss the hydrogen model in more detail and look for further ways of testing this model.

There have been several attempts to give a thermodynamic description of the equilibrium, which this work extends.[1,6–10] In undoped *a*-Si:H, Smith and Wagner assume that only neutral defects equilibrate, and have approached the calculation of equilibrium densities by including a distribution of weak Si—Si bonds which they equate to the valence-band density of states.[9] Doped *a*-Si:H requires a different analysis because the defects are charged and there are also dopant states.[1,7] We base our description on the defect compensation model of doping,[10] and the same approach has been taken by Muller *et al.*[7] The analysis is extended here to account for the

temperature dependence of the transport data in more detail. In fact, we are able to explain from first principles many of the observations of equilibrium and doping that are found in n-type a-Si:H.

The main purpose of this paper is therefore to investigate further the microscopic mechanisms of the equilibrium. The procedure is first to deduce the changes in the density of states from the experimental data using numerical modeling. The same modeling approach is then used to calculate from first principles the equilibrium state by minimizing the free energy. Lastly, we relate the electronic equilibrium to the underlying bonding changes. The paper is therefore organized as follows. In Sec. II new data are presented that further characterize the equilibrium state and the associated changes in the density of states. In Sec. III we describe the modeling procedure and show that a simple density of states leads to an excellent description of the equilibrium, so that we can describe the changes that occur in some detail. The success of the modeling also provides further improvement in the model density of states. Section IV develops a model for the equilibrium in terms of the thermodynamics of the electronic states starting from both an analytical and numerical approach. Section V presents new data on the time-dependent relaxation to equilibrium, and argues for the role of hydrogen. Finally, Sec. VI considers how hydrogen might determine the equilibrium, and also discusses some of the unresolved issues.

II. MEASUREMENTS OF THE ELECTRONIC EQUILIBRIUM

The specific measurements used here to characterize the equilibration are the density of shallow states, n_{BT}, which is obtained from sweep-out experiments,[13] the density of deep states from photothermal deflection spectroscopy (PDS) and C-V characteristic measurements,[14] and the d.c. conductivity. As in previous work, the interpretation of the results is based on a model for doped material, in which dangling bonds are the only significant deep electronic states, so that by charge neutrality,

$$n_{BT}=N_{donor}-N_{DB}\ , \tag{1}$$

where N_{donor} and N_{DB} are the densities of donors and dangling bonds.

The samples are all grown by plasma decomposition using depositions that are known to give good electronic properties (low rf power, pure silane, and a substrate temperature of 230 °C). Virtually all the measurements are for n-type samples which are made by gas phase doping with PH_3.

Figure 1 shows a set of relaxation data for n_{BT} which are more complete than previous results. Initially, the sample is heated to 210 °C for 10 min to bring the structure into equilibrium. The sample is then cooled rapidly in air (rate 2–5 °C/sec) to room temperature, which freezes in a nonequilibrium state. For the room-temperature relaxation, the sample is then measured after resting in the dark for an increasingly long time. For most of the data at elevated temperatures, the sample is annealed in air in an oven for increasing periods, and then cooled to room temperature for measurement. As the data in Fig. 1 show, there is essentially no relaxation at room temperature for times up to an hour, so that the few minutes that the samples are cooled for measurement do not influence the relaxation curves for the higher temperatures. When the temperature is over 100 °C, the relaxation time is so short as to be comparable with the thermal time constant of the oven, and instead the samples were annealed by immersing in hot ethylene glycol.

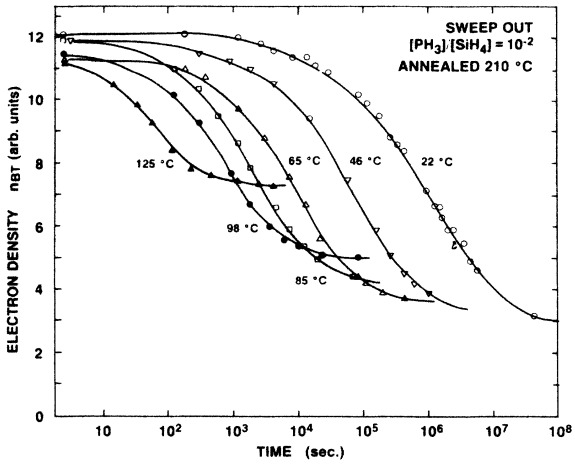

FIG. 1. The relaxation of n_{BT} in an n-type sample at different temperatures following quenching from 210 °C.

It is evident from Fig. 1 that the steady-state value of n_{BT} increases with temperature. More complete data for the temperature dependence of the equilibrium values of n_{BT} are shown in Fig. 2 for two n-type doping levels. (Note that n_{BT} is the charge in the band tail, not the

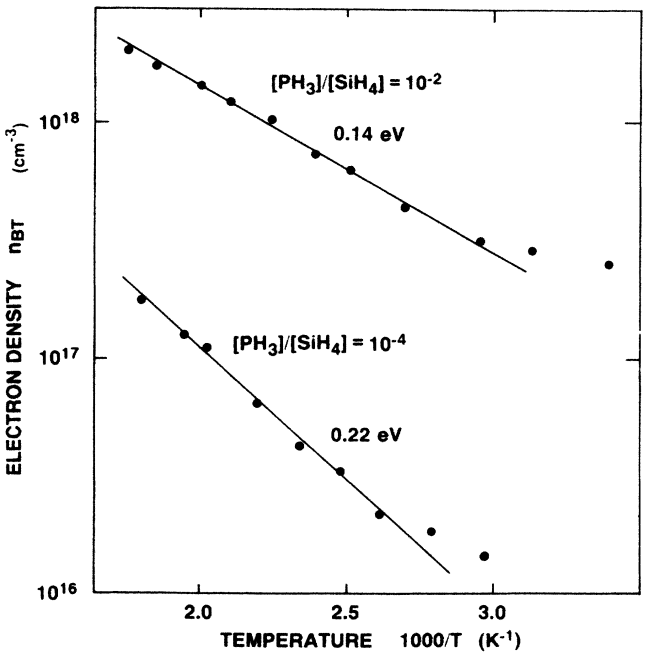

FIG. 2. The temperature dependence of the equilibrium value of n_{BT} in n-type a-Si:H at two doping levels.

free-carrier concentration.) The low-temperature data (<130 °C) are obtained from relaxation curves as in Fig. 1. In this range the sample must be annealed for a sufficiently long time to ensure that it has reached a steady state. At higher temperatures the necessary annealing times are quite short, and a few minutes is sufficient. However, the problem is to ensure that the cooling rate is fast enough to freeze the structure at the configuration of the annealing temperature. Previously, we reported that n_{BT} did not increase above about 200 °C because the cooling rate for an air quench was insufficient.[1] For the measurements here, quenching from temperatures above 180 °C was in cold water, which increases the cooling rate by 1–2 orders of magnitude, and as a result n_{BT} increased up to anneal temperatures of at least 300 °C. It is difficult to confirm that the effective equilibration temperature is indeed equal to the anneal temperature in this range, but the fact that n_{BT} keeps increasing suggests that this is a reasonable assumption. The measurements show that n_{BT} is activated with a fairly small activation energy of 0.14 eV at a doping level of $10^{-2}[PH_3]/[SiH_4]$, increasing to 0.22 eV at $10^{-4}[PH_3]/[SiH_4]$. Near room temperature there seems to be a small departure from the activated form in the one case when careful measurements have been made. Overall, n_{BT} changes by about an order of magnitude over the accessible range of anneal temperatures. For doping levels of 10^{-4} and 10^{-2} the measured dangling-bond densities are approximately 3×10^{17} and 3×10^{18} cm^{-3}, respectively, so that n_{BT} ranges from about 5% to 50% of the dangling-bond density.

A. Changes in the density of states

Although there is now much information about the thermally induced variations in n_{BT}, much less is known about the underlying changes in the density of states $N(E)$. According to Eq. (1), an increase in n_{BT} could occur either through a reduction in N_{DB} or an increase in N_{donor}, or by changes in both quantities. In order to explore the thermally induced changes in N_{DB} and N_{donor}, photothermal deflection spectroscopy (PDS), capacitance-voltage (C-V) characteristics, and bias-annealing measurements have been performed on samples annealed and quenched at different temperatures. The results of the PDS experiments are shown in Table I. The sample had a doping level of $10^{-2}[PH_3]/[SiH_4]$ and a dangling-bond density of $\sim3\times10^{18}$ cm^{-3}. The relative changes in the defect density were found by taking the ratio of the PDS spectra after different annealing conditions and comparing the subgap region of defect absorption with the band-edge region. The procedure allows changes of about 10% in the defect density to be detected. As is seen from the results in Table I, over a wide range of accessible equilibration temperatures, corresponding to quenching in water from 240 °C or annealing for 2 h at 130 °C, there is no discernible significant change in N_{DB}, compared to the initial state of the sample which had been rested at room temperature for several months. In the data of Fig. 2, the largest n_{BT} is about 50% of the dangling-bond density and the smallest is $\sim20\%$. The absence of any detectable change in N_{DB} therefore suggests that variations in the donor density must account for the increase in n_{BT}, and this result is confirmed by the experiment described next.

The changes in $N(E)$ were also investigated by sweep-out measurements of n_{BT} after bias annealing. Previously it was shown that annealing and quenching under reverse bias resulted in a large increase in n_{BT}, compared to quenching without bias.[15] The effect is similar to that reported by Lang *et al.* from capacitance results.[16] Our explanation is that a depletion bias perturbs the electronic equilibrium by depressing the Fermi energy and changing the occupancy of the states. The charge neutrality expression is then given by

$$n_{BT}(\text{bias})=N_{donor}-N_{DB}-Q_{depl}/wq\ , \tag{2}$$

where Q_{depl} is the depletion charge induced by the bias, w is the width of the n-type layer, and q is the electronic charge. Equilibrium is regained by changes in N_{DB} and/or N_{donor} which restores the usual value of n_{BT}. However, when the bias is removed n_{BT} increases by Q_{depl}/wq. The results in Fig. 3 are for an n-type sample doped $10^{-5}[PH_3]/[SiH_4]$. The sample has a particularly thin n-type layer so that the normal equilibrium sweep-out charge (qwn_{BT}) is small. As the bias annealing is performed at higher temperatures, and for longer times, the resulting n_{BT} increased by nearly 2 orders of magnitude up to a density of 4×10^{17} cm^{-3}. Even this high value does not represent the ultimate steady state, but instead is limited by current injection at the contact since the field at the contact increases as the depletion charge increases. Because of this limitation, the largest bias-annealing effects in n_{BT} occur in samples with the thinnest n-type layers. We note that related bias-annealing effects have been seen in solar cells.[17] An improvement in the efficiency is found which is consistent with an enhancement of the doping efficiency of p or n layers.

The highest measured n_{BT} value of 4×10^{17} cm^{-3} should be compared with the usual equilibrium value of less than 10^{16} cm^{-3} and the normal densities of donors and dangling bonds which are both about 10^{17} cm^{-3}. Thus even if N_{DB} decreased to zero, N_{donor} must increase by a factor 4 to account for the results, demonstrating that the donor states definitely participate in the equilibration. A gas phase doping of 10^{-5} corresponds to a bulk phosphorus concentration of $\sim10^{18}$ cm^{-3}, when the enhancement factor for incorporation is included. The

TABLE I. Results of PDS measurements of the defect density in a sample doped $10^{-2}[PH_3]/[SiH_4]$ after annealing at different temperatures, compared to the rested state.

	Rested	$T_A=130$ °C	$T_A=190$ °C	$T_A=240$ °C
N_{DB}(relative)	1.0	0.95	1.01	0.98

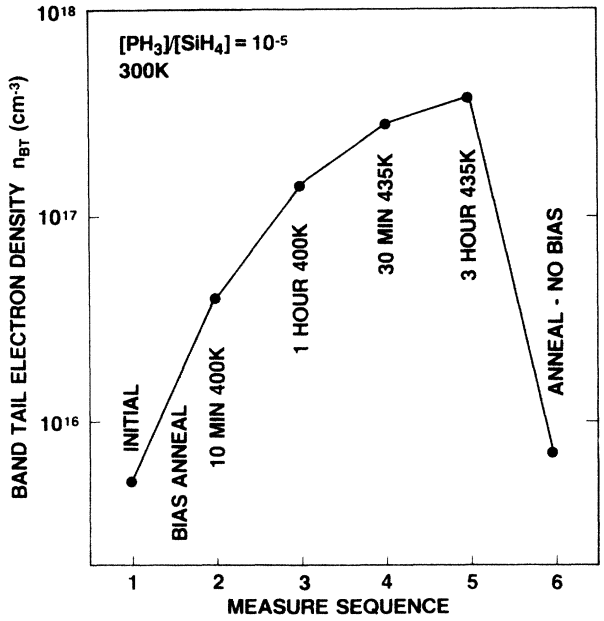

FIG. 3. Measurements of n_{BT} after bias annealing, showing the enhancement of the electron density by nearly 2 orders of magnitude.

bias-annealing results therefore show that the doping efficiency reaches about 40% and possibly could go even higher.

Capacitance-voltage measurements at a range of frequencies are the third experiment used to study the changes in the density of states as a result of equilibration. The capacitance C of an n-type sample measures the width of the depletion layer, and as a reverse bias V is applied, the depletion layer broadens. (Note that the measurements are at room temperature, so that the sample is in the frozen state and the bias does not change the doping efficiency.) It is observed that samples quenched from a higher temperature have a greatly increased capacitance, clearly due to the higher electron density induced by annealing which results in a lower depletion-layer width. In a crystalline semiconductor with discrete levels, a plot of $1/C^2$ against V can be directly related to the density of dopants. The analysis of the data in an amorphous semiconductor is more complicated because of the broadened energy levels, and instead we use a numerical calculation using the known distribution of states, as is described elsewhere.[14] At low bias, the depletion width is mostly determined by the shallow states, and so is most sensitive to the changes in n_{BT}, whereas at high bias the deep states are also important, so that the changes in both types of states can be deduced. Table II shows typical results from one sample and compares the rested state with the result of annealing and quenching at a different high and a low equilibration temperature. The donor density increases significantly with anneal temperature, while the change in the dangling-bond density is smaller. The capacitance results therefore confirm the conclusions of the PDS and bias-annealing experiments.

If it is assumed that the temperature dependence of

TABLE II. Band-tail charge, dangling bond density, and donor density (cm^{-3}) for 10 ppm phosphorus doped sample as obtained from C-V data at 100 KHz.

State	Rested	$T_A = 65$ °C	$T_A = 250$ °C
N_{BT}	3×10^{15}	9×10^{15}	4×10^{16}
N_{DB}	8×10^{16}	9×10^{16}	9×10^{16}
N_{donor}	8.3×10^{16}	1.0×10^{17}	1.3×10^{17}

N_{DB} is activated, as might be expected for a thermal equilibrium process,

$$N_{DB} = N_0 \exp(-E/kT) , \quad (3)$$

then it is clear from the results of Tables I and II that the energy E must be close to zero. Any model for thermal equilibrium must account for the low values of E, and this point is discussed in greater detail later.

III. MODELING OF THE ELECTRONIC EQUILIBRIUM

A. Modeling procedures

The aim of the modeling is to relate the observed equilibration effects in the sweep-out and conductivity data to the underlying changes in the density-of-states distribution. Two types of calculations are made. First we use the modeling to relate the different experimental results, for example, the sweep-out and the dc conductivity. Then we derive the equilibrium configuration from free-energy considerations. The density of states used in the calculations is shown in Fig. 4, which depicts the upper half of the band gap for n-type samples. The model is based on a variety of measurements that have explored the different features of the density of states, but it must be recognized that the full distribution has not been experimentally verified. The upper part of the conduction band is derived from the inverse photoemission re-

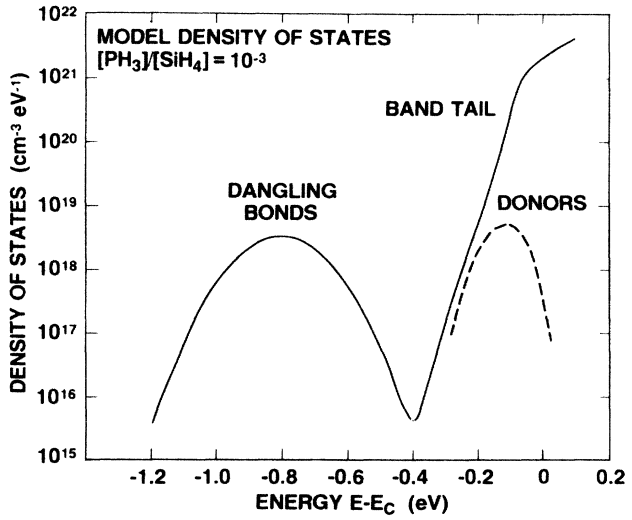

FIG. 4. The density-of-states model used for the numerical calculations of the electronic properties. The dangling bond and donor peak magnitude vary according to the doping level.

sults of Jackson *et al.*,[18] which find a linear energy dependence in the region of the mobility edge. Further into the gap, an exponential band tail is assumed with a slope corresponding to a characteristic temperature T_C of 260 K, as found in drift mobility experiments on our samples.[19] The mobility edge E_C is located at a density of states of 2×10^{21} cm^{-3}eV^{-1}, as we have used previously and in general agreement with the inverse photoemission results. In this position, E_C lies about 0.1 eV above the exponential region of the band tail. This shape for the band edge is quite similar to that deduced by Spear, except that the overall density is higher.[20] The dangling-bond peak is located at E_d, 0.8 eV below E_C as observed in deep-level transient spectroscopy (DLTS),[21] and we assume a Gaussian shape for the defect band, usually with a width of 0.15 eV which is close to the measured value. Other DLTS data give similar results and also provide direct evidence for the deep minimum in the density of states at about $E_C-0.4$ eV.[22] Since the defect band is invariably almost full in n-type material, we only consider the upper Hubbard band, corresponding to the negative state. The donor band has the least precisely known distribution, and is assumed to be Gaussian with its peak position 0.05–0.2 eV below E_C with a width of about 0.1 eV. As is shown below, the modeling is able to place some limits on its position.

The electronic configuration is completely defined by the density of states, the total density of electrons, and the temperature. The modeling procedure is to first assume a total density of donors and dangling bonds, and a set of shape parameters that completely determines the shape of the density of states. A trial Fermi energy is chosen and the electron distribution is calculated for a particular temperature using full Fermi statistics. The model is tested for charge neutrality, the condition being equality between the total density of electrons and donors. The position of E_F is then adjusted until neutrality is obtained. While most calculations are made with the density-of-states parameters as described above, we have also varied the shape of the dangling bonds, the tail states, and the donors to explore the sensitivity of the results to the various parameters.

B. Equilibrium conditions

In earlier work it was argued that in equilibrium, the Fermi energy is at the density-of-states minimum between the band tail and the dangling-bond level, and does not change with temperature. The numerical modeling allows us to check whether this is indeed so. Figure 5 shows calculations of the temperature dependence of the Fermi energy for different doping levels, based on the n_{BT} data in Fig. 2. At the 10^{-2}[PH$_3$]/[SiH$_4$] doping level, N_{DB} is known to be about 3×10^{18} cm^{-3} (Ref. 23) and an order of magnitude lower at 10^{-4}[PH$_3$]/[SiH$_4$]. Thus at each temperature we use the appropriate values of N_{DB} and the measured n_{BT} to obtain N_{donor}, and the calculation then finds the position of E_F. It is seen that over the range of 300–580 K, E_F is only weakly temperature dependent with a slope of $(0-2)k$. Note that the experimental uncertainty in the measurement of n_{BT} tends to overestimate the temperature dependence. Incomplete relaxation makes the measured n_{BT} too high at low temperature, and insufficiently fast cooling makes it too low at high temperature.

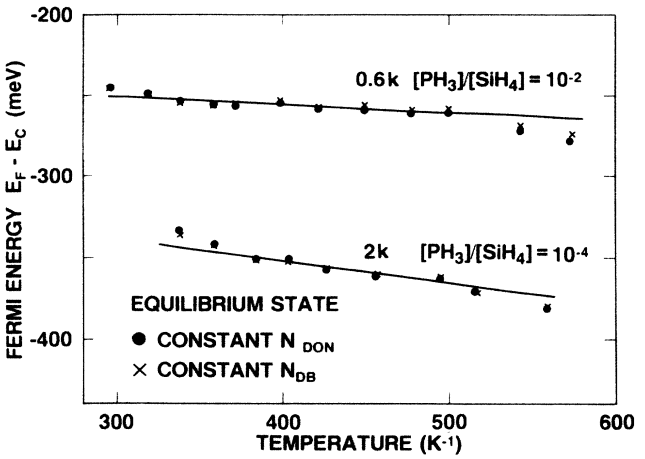

FIG. 5. The calculated temperature dependence of the Fermi energy in equilibrium at two doping levels, derived from the sweep-out measurements in Fig. 2.

These calculations assume a constant N_{DB} and varying N_{donor} with temperature as indicated by experiment. In fact, it is not clear exactly how N_{donor} and N_{DB} vary independently in equilibrium, without invoking thermodynamics in the way described later in the paper. The calculations of E_F were therefore repeated keeping N_{donor} fixed and finding N_{DB} from the known n_{BT}. As seen in Fig. 5, the results are practically identical, showing that the modeling of E_F is insensitive to the uncertainty in the underlying behavior. The reason is that E_F is almost entirely determined by the magnitude of n_{BT}, and the density of states above the minimum of $N(E)$. Since the donor band is mostly hidden within the intrinsic band tail, small changes in N_{donor} have little influence on the results.

The modeling therefore confirms that E_F does not vary strongly with temperature in equilibrium, as was assumed in our previous analysis. On the other hand, the position of E_F, particularly at the higher doping level, is closer to the conduction-band edge rather than being at the minimum of the density of states as depicted in Fig. 4. It is unclear whether this represents a significant departure from our previous model, because the position of the minimum will be shifted if the actual width of the dangling-bond band or the slope of the band tail is different from our assumed values and these parameters are not very accurately known.

Once the position of E_F has been obtained, the temperature dependence of the dc conductivity is readily deduced. It is assumed that conduction takes place above the mobility edge and is given by

$$\sigma = n(E > E_C) e \mu_{\text{free}} , \tag{4}$$

where $n(E > E_C)$ is the density of electrons above E_C, and μ_{free} is the free-carrier mobility, taken to be 10 cm^2/V sec. The points in Fig. 6 show the calculated conductivity for the 10^{-2} and 10^{-4}[PH$_3$]/[SiH$_4$] doping lev-

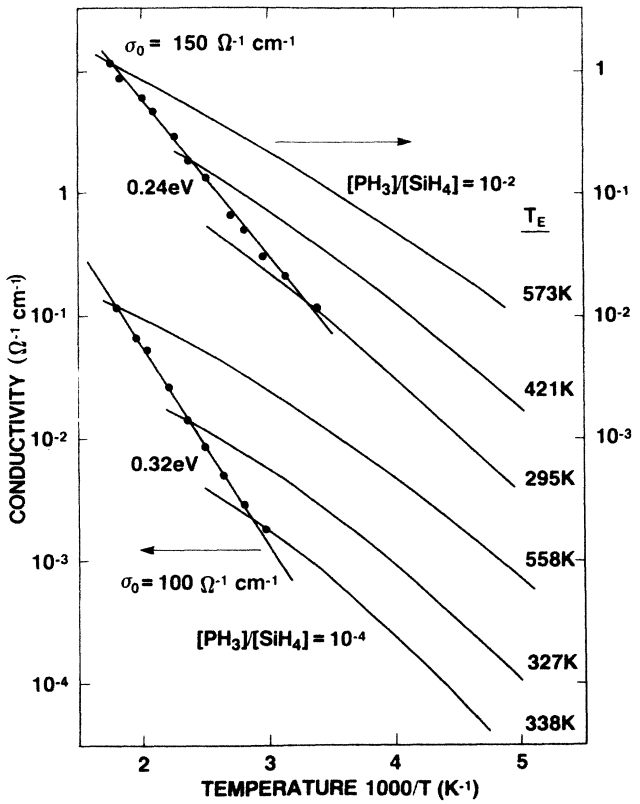

FIG. 6. The calculated conductivity at two doping levels for both the equilibrium and the frozen-in states, based on the sweep-out data of Fig. 2. The points are calculated from actual n_{BT} data. The assumed equilibrium temperatures for the frozen-in state are shown.

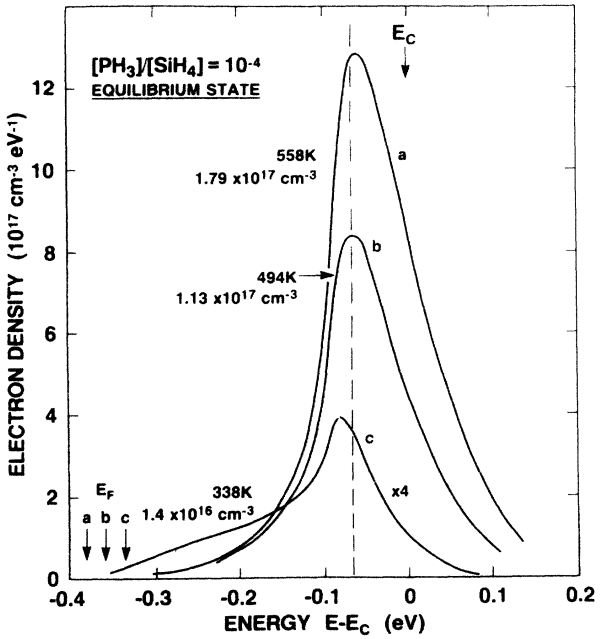

FIG. 7. The calculated band-tail electron distribution based on measured n_{BT} values, showing that above room temperature, the electrons occupy a fairly narrow peak 0.05–0.1 eV below the mobility edge.

el, derived from the n_{BT} data. The activation energies (0.24 and 0.32 eV) and prefactor of 100–150 $\Omega^{-1}\,cm^{-1}$ agree extremely well with the measured data (0.28 and 0.34 eV, 200 $\Omega^{-1}\,cm^{-1}$).[5] The fact that we can take the n_{BT} data and accurately calculate the conductivity is good confirmation that both the model density of states and the position of E_F are essentially correct. The agreement with experiment would be improved by a slight shift of the assumed mobility edge position to higher energy by ~20 meV, but the results are within the experimental uncertainty of the data.

It is of interest to note that both n_{BT} and σ, are activated, but with different energies of 0.22 and 0.34 eV, respectively, for 10^{-4} doping (compare Figs. 2 and 6). Figure 7, which shows the temperature dependence of the electron distribution, illustrates the origin of the different energies. These calculations are made for the 10^{-4} doping level and use the n_{BT} data in Fig. 2 to calculate E_F at different temperatures. The occupied band-tail-state distribution is then calculated from the density of states and the Fermi function. The results illustrate that the electron distribution peaks well above E_F because $N(E)$ in the band tail increases more rapidly than the decrease of the Fermi function when the temperature is above the 260-K slope of the tail. The peak of the electron distribution varies a little with temperature, and lies 50–100 meV below E_C, and this is the origin of the difference between n_{BT} and σ. The peak in the electron density occurs at the energy where the density-of-states distribution becomes flatter at the top of the exponential tail. If the exponential tail continued up to the mobility edge, then the two activation energies for n_{BT} and σ would be the same. The difference of ~0.1 eV is a clear demonstration that E_C occurs beyond the range of the exponential tail.

C. Nonequilibrium conditions

In the frozen-in state, the density of states and hence n_{BT} are independent of temperature, but reflect the equilibrium values at some higher temperature from which the sample has been quenched. This leads to a very different temperature dependence of the Fermi energy compared to the equilibrium case. The calculations are for the same doping levels as in the equilibrium case (10^{-2} and 10^{-4}). To model the freezing of the structure from different temperatures, we hold n_{BT} and the density of states constant at the values corresponding to a particular equilibration temperature, and then calculate the temperature dependence of E_F, which is shown in Fig. 8. E_F now varies much more rapidly with temperature than for the equilibrium case, having a slope of up to $9k$.

The difference between the equilibrium and nonequilibrium conditions are now very apparent. In the frozen-in state, there is a strong statistical shift of the Fermi energy, with E_F moving by up to 100 meV between 200 and 400 K. The shift of E_F causes a reduction in the effective activation energy E_a, and also of the conductivity prefactor σ_0, where

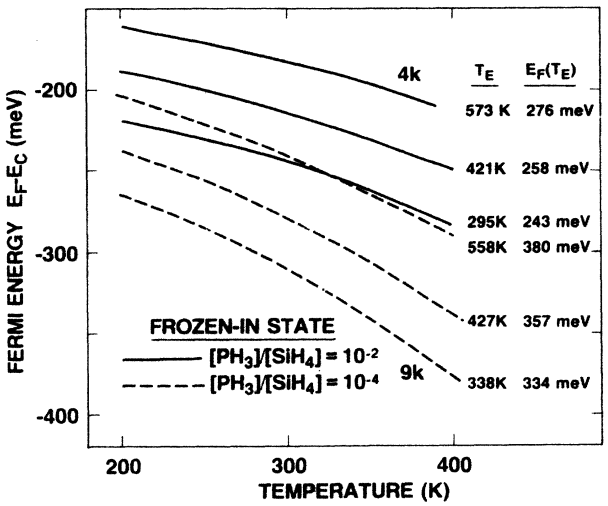

FIG. 8. The calculated temperature dependence of the Fermi energy for the frozen-in state and for different equilibration temperatures.

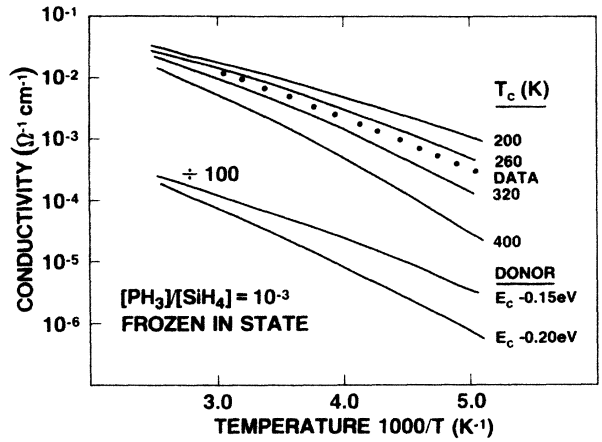

FIG. 9. Calculations of the temperature dependence of the conductivity in the frozen-in state, showing the influence of different assumed slopes of the band tail, and positions of the donor band.

$$\sigma = \sigma_0 \exp(-E_a/kT) , \tag{5}$$

Figure 6 shows the calculated temperature dependence of the conductivity in the frozen state and in equilibrium. Each curve for the frozen state corresponds to freezing the structure from the indicated temperature, and is based on the value of n_{BT} measured at that temperature. The difference between a strongly temperature dependent E_F in the frozen-in state, and an almost temperature independent E_F in equilibrium, results in different slopes for the calculated conductivity, as is observed experimentally.[1,5] The calculations also show that as the freezing temperature decreases, the model predicts that the conductivity drops, and its activation energy increases. These results are in excellent agreement with the data.

The meaning of these different conductivity curves is as follows. When a sample in equilibrium is subject to a temperature change, the conductivity will follow a trajectory that lies between the two extremes that we have calculated and shown on Fig. 6. An extremely slowly varying temperature allows the sample to remain in equilibrium, resulting in the observation of the larger activation energy. A very rapid change of temperature prevents equilibration and the smaller activation energy is seen. For experiments in which a sample is rapidly quenched and then slowly warmed, σ will first follow the frozen-in curves, then will drop towards the equilibrium curve as the equilibration temperature is approached, and finally will follow the equilibrium curve. These effects are all observed.[1,5]

Figure 9 shows further calculations of the conductivity in the nonequilibrium regime, as various density-of-states parameters are varied. For example, as the slope of the conduction-band edge is increased from 200–400 K, the activation energy decreases by about 50%, for a constant value of n_{BT}. The calculated conductivity is also weakly dependent on the position of the donor band.

The model calculations are therefore in good agreement with the experimental observations for the frozen-in state as well as in equilibrium. We can reproduce the activation energy and prefactor very well with the same parameters that fit the equilibrium case, and the trends with changing n_{BT} are obtained. The only discrepancy is that the model gives a small but significant downward curvature in the temperature dependence of the conductivity for the frozen state (see Fig. 6), whereas the measurements show a single activation energy or sometimes an upward curvature. The curvature in the model calculations is a consequence of the general shape of the band tail, and cannot be removed by any simple modification of the density of states. We believe that the discrepancy with the data is probably because it is an oversimplification to assume that conduction occurs above a fixed mobility edge. Monroe has shown that there is a significant contribution to the conductivity by hopping below E_C, and that this contribution increases as the temperature is lowered.[24] The effect is to give a low-temperature conductivity which is larger than that calculated by our model, which would tend to straighten out the temperature-dependence data. In addition, near the equilibration temperature the slow time dependence of n_{BT} causes a distortion of the conductivity data, which also influences an exact comparison of data and model.

D. The donor band

The preceding model calculations assume a donor band 0.1 eV below E_C, and with a width of 0.1 eV. The results are, in fact, fairly insensitive to the choice of these parameters, so long as the donor band remains largely hidden within the band tail, so that the conductivity and n_{BT} data do not give much information about the donors. However, the hyperfine interaction in ESR can distinguish between electrons occupying the intrinsic band-tail states, and those occupying donors.[25] We have therefore used the model to fit these data, to obtain limits on the donor band parameters. As in crystalline silicon, the neutral donor density decreases at elevated temperatures because electrons are thermally excited into the

conduction-band tail. A complication in the data is that although the silicon band-tail resonance increases with temperature as expected, the total spin density decreases slightly. The proposed explanation was that electrons excited near the conduction band have such a short lifetime that the resonance is greatly broadened out.[25] The effect is not too large—the total spin density drops by 20% by 300 K—but this uncertainty limits the precision of the modeling results. We assume that both ESR resonances are affected similarly, and therefore fit the fraction F_D of the total ESR signal that originates from the hyperfine split lines. In addition, there are reported data for the doping dependence of F_D,[25] measured at low temperature, and these are replotted in Fig. 10.

Examples of the fits are shown in Fig. 10 for different parameters. The total donor concentration is known from the doping level. No one set of parameters gives an accurate fit to both the temperature dependence and the doping dependence, but the trends are reproduced fairly well. As would be expected, F_D increases with the width of the donor band and with the binding energy. The best fit to the doping dependence is with a binding energy of 50 meV and a width of 150 meV. A slightly worse fit is obtained by using 100 meV for both parameters, and a significantly deeper donor gives a much poorer fit. Both sets of parameters give the same calculated temperature dependence which has the correct general shape, but is not a particularly good fit to the data. It seems likely that the donor band may change shape with doping concentration, and also probable that it has an exponential rather than Gaussian low-energy tail. However, given the limited data it did not seem valuable to explore these possibilities further.

IV. THEORY OF THE ELECTRONIC EQUILIBRIUM

The electronic equilibrium is defined by the density of states, the electron occupancy, the position of E_F, etc. In this section we develop a model based on free-energy minimization to account for the experimental results and to determine the relation between phosphorus incorporation, and dangling bonds and donors. It is useful to begin by summarizing the information to be explained by any theory.

(1) Shallow occupied states. In equilibrium, n_{BT} increases with temperature, with an activation energy of 0.1–0.3 eV, depending on doping, with a total change of about an order of magnitude over the measured temperature range of 25–300 °C.

(2) Dangling bonds. Most models of equilibrium assume that the density of dangling bonds varies with temperature. Certainly, the variation of n_{BT} implies that either N_{DB} or N_{donor} (or both) are temperature dependent. Our present data indicate, however, that N_{DB} is almost unchanged with temperature.

(3) Donors. Again, a temperature-dependent donor density is implicated by the n_{BT} data and Eq. (1). The experiments described in Sec. II A indeed point to an increase in N_{donor} with temperature and with bias annealing, with changes of about a factor 2 from 60 to 250 °C.

(4) Band-tail distribution. Time-of-flight measurements find no change in the hole drift mobility with equilibration temperature, at least for p-type and undoped samples, from which we conclude that the shape of the valence-band tail is not influenced significantly by the equilibration.[11,26] We are assuming that the same is true of the conduction band.

(5) The Fermi energy. Modeling has shown that E_F is almost independent of temperature in equilibrium, and lies near the minimum of $N(E)$ between the dangling-bond band and the band tail.

A. Analytical model

Our analysis of the equilibrium effects begins with an idealized version of the defect compensation model of doping.[10] This model assumes that donors and dangling bonds are in equilibrium, and as shown before by ourselves and Muller *et al.*,[1,7] is able to explain the general features of the data. It is useful to analyze this model in more detail, which is done as follows. In order to have an analytic solution, we assume that the donors and dangling bonds reside in discrete energy levels at E_p and E_d, as shown schematically in Fig. 11. The band tail is represented by a large density of states N_T also located at E_p, and we do not include the conduction band at all. The formation energies of *neutral* donors and *neutral* dangling bonds are taken to be U_p and U_d, respectively. Since the states are charged, the actual formation energies depend on the position of the Fermi energy E_F, being $U_p - E_p + E_F$ for the donors, with a similar expression for dangling bonds. The total free energy is then written as

$$F(f_p,f_d)=N_p f_p(U_p-E_p+E_F+kT\ln f_p) + N_0 f_d(U_d-E_F+E_d+kT\ln f_d)\,. \quad (6)$$

Here, f_p and f_d are the fraction of the available states, of density N_p and N_0, that are donors and dangling bonds. Thus N_p might be the total phosphorus density, and N_0 the total silicon density, although the actual values are discussed below. The entropy terms proportional to $\ln f$, are the same as used by Smith and Wagner[9] and are based

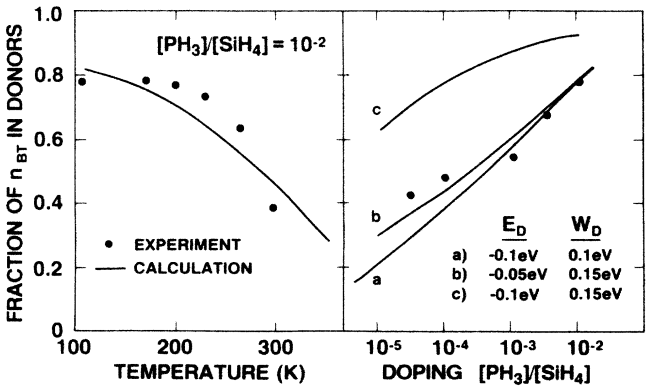

FIG. 10. A comparison of the measured fraction of band-tail electrons that occupy the donor states at different temperatures and doping levels, with the calculated values based on different choices for the donor band position and width.

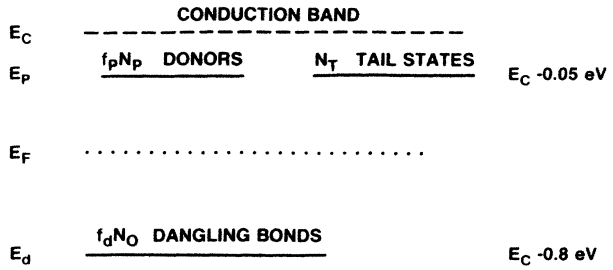

FIG. 11. An illustration of the model assumed for the free-energy minimization.

on a lattice-gas model. The equilibrium condition is then found by minimizing F with respect to both f_p and f_d. These two equations, together with the charge neutrality condition, can be solved for f_p, f_d, and E_F. With substitutions

$$N_{\mathrm{DB}}=N_0 f_d,\quad N_{\mathrm{donor}}=N_p f_p,\quad n_{\mathrm{BT}}=N_p f_p-N_0 f_d \tag{7}$$

and

$$N_p^{-1}\,dE_F/df_p=-N_0^{-1}\,dE_F/df_d=\beta\ ,$$

where β is determined below, we obtain

$$N_{\mathrm{DB}}N_{\mathrm{donor}}=N_0N_p e^{-2}\exp\{-[U_p+U_d-(E_p-E_d)]/kT\}\ . \tag{8}$$

As expected, this analysis reproduces the defect compensation model, and follows directly from the law-of-mass action applied to the reaction

$$\mathrm{P}_3^{\,0}\leftrightarrows \mathrm{P}_4^{\,+}+D^-\ . \tag{9}$$

From Eq. (8), provided U_p and U_d are such that $N_{\mathrm{donor}}\approx N_{\mathrm{DB}}$, we have

$$N_{\mathrm{donor}}\approx N_{\mathrm{DB}}\approx (N_0N_p)^{1/2}e^{-1}\times\exp\{-[U_p+U_d-(E_p-E_d)]/2kT\}\ , \tag{10}$$

thus reproducing the square-root dependence on N_p found for doping.[23] The formation energy U_{tot} for both donor and dangling bond is seen to be

$$U_{\mathrm{tot}}=\tfrac{1}{2}[U_p+U_d-(E_p-E_d)]\ . \tag{11}$$

The energy of the process is half the sum of the individual formation energies minus the energy gained when an electron drops from E_p to E_d, which corresponds to the physical picture of the doping model. Individually the formation energies of donors and dangling bonds are too large to give high densities, but in charged pairs the energy is much lower, allowing doping in the presence of the compensating defects.

The energy-minimization equations also give the Fermi energy position in equilibrium as

$$E_F=\tfrac{1}{2}(E_p+E_d)+\tfrac{1}{2}(U_d-U_p)-\tfrac{1}{2}kT\ln[(N_0/N_p)(1-n_{\mathrm{BT}}/N_{\mathrm{DB}})]-\beta n_{\mathrm{BT}}\ . \tag{12}$$

Within the assumed density of states in Fig. 11, providing $N_T\gg N_{\mathrm{donor}}$, n_{BT} is given by

$$n_{\mathrm{BT}}=N_T\exp[-(E_p-E_F)/kT]\ , \tag{13}$$

from which it is readily found that $\beta n_{\mathrm{BT}}=kT$, so that

$$E_F=\tfrac{1}{2}(E_p+E_d)+\tfrac{1}{2}(U_d-U_p)-kT\{1+\tfrac{1}{2}\ln[(N_0/N_p)(1-n_{\mathrm{BT}}/N_{\mathrm{DB}})]\}\ . \tag{14}$$

Equations (11) and (14) define the equilibrium, giving the density of states and the position of the Fermi energy. Equation (14) illustrates that the position of E_F is determined by the difference in the individual formation energies, in contrast to the density of states which is only dependent on the sum. The first term in Eq. (14) indicates that for equal U_d and U_p, E_F would be pinned midway between the two states, provided the temperature-dependent term is fairly small. If $U_d>U_p$, then E_F moves up toward the band edge. Thus a major contribution to the doping of a-Si:H is from this energy difference. In previous work we argued that E_F was pinned in the density-of-states minimum between the two bands from considerations of the doping model. The present analysis justifies the assumption of a pinned E_F, but that the precise position depends on the formation energies as well as the density of states. Finally, we note that E_F is predicted to have only a weak temperature dependence, but one that depends on the values of N_0 and N_p. [The term $n_{\mathrm{BT}}/N_{\mathrm{DB}}$ in the temperature-dependent part of Eq. (14) is small and can be neglected.]

The physical interpretation of the thermodynamics is that the Fermi energy adjusts to a level that equalizes the formation energies of dopants and defects. For example, suppose that E_F was at a lower energy than given by Eq. (14). The formation energy of the donors ($U_p-E_p+E_F$) would then be reduced so that their density would increase. This effect would then raise the Fermi energy. A corresponding argument applies to the dangling bonds. The weak temperature dependence of E_F therefore comes about because the changes in formation energy tends to cancel out the statistical shift, causing the Fermi energy to be effectively pinned.

The various parameters in the analysis can be roughly estimated as follows. From the density-of-states model in Fig. 4, the energy E_p-E_d is 0.75 eV with the donor level at $E_C-0.05$ eV. It has been argued that the source of defects are the weak Si—Si bonds, rather than every silicon atom.[27,28] It is unclear how many such weak bonds are present, but we guess that this might be about 0.1–1 % of the bonds, and so set N_0 to be 10^{19}–10^{21} cm^{-3}. However, the bias-annealing experiment indicated that the doping efficiency could approach unity, so we set N_p to the total phosphorus concentration. These choices, which are discussed later, imply that at high doping levels, $N_p\sim N_0$, so that the temperature dependence of E_F is very weak, in agreement with the results in Fig. 5. The information that at a doping level of 10^{-3}, the dangling-bond density is 10^{18} cm^{-3}, for growth at 230 °C, then gives a value of U_p+U_d of about 0.9 eV. On the other hand, the measured position of E_F gives U_d-U_p of about

0.3 eV, resulting in an estimated defect energy of 0.6 eV and for donors of 0.3 eV. In undoped a-Si:H, the density of neutral dangling bonds is $10^{15}-10^{16}$ cm^{-3}. Assuming that these defects are in equilibrium at the growth temperature of 230 °C yields a formation energy of about 0.5 eV, which is close to the above estimate. Thus a consistent and plausible set of parameters accounts for the results.

B. Numerical model

The analytical model accounts well for the general features of the equilibrium state. However, it is based on an oversimplified density-of-states distribution, which might influence the results. We have therefore repeated the energy-minimization procedure by numerical calculation using the actual density of states which was applied to the modeling of the transport. The procedure starts with an initial guess at N_{DB} and N_{donor}, calculates E_F using the full density of states, and then calculates the free energy from Eq. (6). The free energy is then minimized by successive iterations. We still assume a single value of the formation energy for defects and donors, and so are not including any distribution of sites, nor any dependence on the energy level in the gap. These assumptions are discussed later.

Figures 12–14 illustrate the results obtained by the free-energy minimization. Figure 12 shows the temperature dependence of E_F for different assumed values of U_d and U_p, and compares the results with those obtained from the analytical model [Eq. (14)]. For the calculations we take $N_0=10^{19}$ cm^{-3} and plot results for a doping level of 10^{-3}. The broadened density of states tends to push E_F towards the minimum in the density of states compared to the analytical model. The reason is that the neutral states are energetically unfavored, so that when E_C-E_F is small the numerical model gives a lower position of E_F. On the other hand, when E_F is into the defect band, the numerical model gives a higher E_F. The results in Fig. 12 show that the full density of states also changes the temperature dependence of E_F. Again E_F is pushed towards the density-of-states minimum at elevated temperatures because of the tendency to minimize the density of the neutral states. The analytical solution is therefore not a particularly good approximation, although both calculations give only weak dependences, at least at high doping levels. At lower doping levels a stronger temperature dependence is expected due to the $\ln(N_0/N_p)$ term in Eq. (14). The calculations are for a doping level of 10^{-2}, which has a measured activation energy of 0.28 eV, so that the best fit is obtained with $U_d=0.6$ and $U_p=0.3$ eV in agreement with the analytical model, and these parameters are therefore used in the remaining calculations.

Figure 13 shows the calculated temperature dependence of the dangling-bond density and n_{BT} based on the best choice of parameters from Fig. 12. The defect density follows a square-root dependence on doping, in agreement with experiment, with approximately the correct density of 10^{17} cm^{-3} at a doping level of 10^{-5}, and 3×10^{18} at 10^{-2}. The dangling-bond density is activated with a small energy of less than 0.1 eV, rather than being independent of temperature, and this is a point discussed further below. n_{BT} also has an approximate square-root dependence on doping, with about the correct magnitude. The activation energy of about 0.15 eV is given correctly for the highest doping level (compare Fig. 2), but is a little too low at the lower doping levels.

In Fig. 14 the calculated dc conductivity is plotted assuming a free-carrier mobility of 10 cm^2/V sec and compared to experimental results. The calculations come very close to reproducing the measured doping depen-

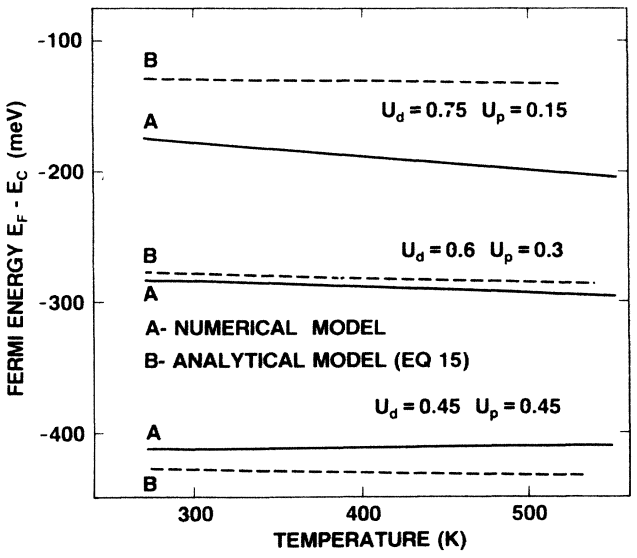

FIG. 12. The calculated temperature dependence of the Fermi energy from the numerical free-energy minimization model compared with the analytical model of Eq. (14). A weak bond density of 10^{19} cm^{-3}, and a doping level of 10^{-2}[PH$_3$]/[SiH$_4$], is assumed.

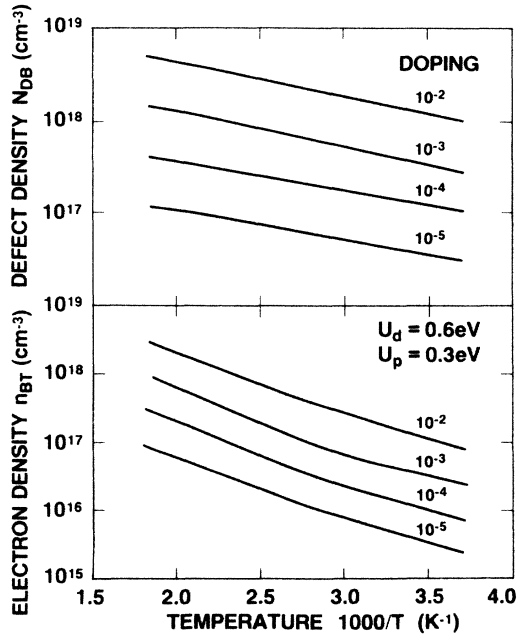

FIG. 13. Calculated temperature dependence of the dangling-bond density (upper) and n_{BT} (lower) for different doping levels using the same model parameters as in Fig. 12.

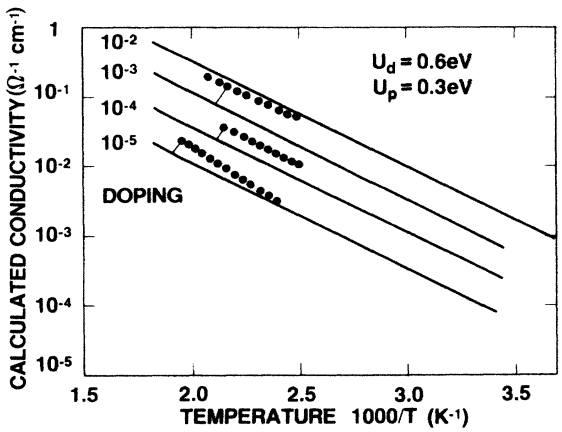

FIG. 14. Calculated thermal-equilibrium dc conductivity from the free-energy minimization model compared to the experimental results of Ref. 1.

dence. The activation energy is about right at high doping levels, although it does not increase at lower doping as much as the experiments indicate. It is therefore very satisfactory that with a simple model we can compute, essentially from first principles, virtually all the electronic properties of doped a-Si:H, and obtain reasonable agreement with the observations. This leads us to conclude that the free-energy minimization model is essentially correct.

There are, however, two aspects of the calculations that do not fully agree with the experimental results. In the model, both n_{BT} and σ increase with the doping level, but with little change in their activation energies, whereas experimentally a small but significant change in the energy is observed. This result comes about because the model gives too large a temperature dependence of E_F at low doping levels. This is apparent from Eq. (14) in which E_F contains the term (approximately) $kT\ln(N_0/N_p)$ which obviously gets larger as N_p decreases. A better fit to the data would result from a choice of the density of weak bonds, N_0, which increased with doping. The other difference between model and experiment is the temperature dependence of N_{DB}. In Tables I and II evidence is presented that N_{DB} is essentially independent of temperature in equilibrium. It is easy to see from Eqs. (10) and (11) that this can only be explained by the model if the energy $U_{tot} \approx 0$. The density of dangling bonds should then approach the density of accessible states, so that a very low value of N_0 must be assumed to get the correct temperature dependence. A possible alternative explanation is that most or all of the dangling bonds do not in fact participate in the equilibration, but this seems unlikely given the evidence for equilibration of the defects in undoped a-Si:H.[3,4]

The differences between model and experiment seem to be related to the choice of N_0, and this is the parameter that is the most uncertain since it depends on the detailed microscopic mechanisms of defect creation. In the next section and in the discussion we argue that our assumption of a constant N_0 and a single formation energy is a severe oversimplification which may be the origin of the remaining differences between model and experiment.

V. THE STRUCTURAL RELAXATION TOWARDS EQUILIBRIUM

The fact that a-Si:H attains equilibrium implies that there must be bonding rearrangements that cause the changes in the density of states. There must also be an energy barrier for these structural rearrangements which is manifested in the electronic properties as the temperature-dependent relaxation times. We therefore study the time-dependent relaxation from a nonequilibrium state towards equilibrium in order to obtain information about the structure.

A. The role of hydrogen

Previously, we proposed that the structural changes are caused by hydrogen motion, although descriptions of the equilibrium based only on rearrangements of the silicon network have also been proposed.[8] The main evidence for the role of hydrogen was that diffusion occurs in the same temperature range as the equilibration. Furthermore, by relating the diffusion coefficient to the effective viscosity at the equilibration temperature, the diffusion rate quantitatively accounts for the equilibration times. There is now additional evidence for the role of hydrogen in the equilibration, as follows.

In Fig. 1 the time-dependent decay of n_{BT} from its initial high value to an eventual steady state is seen. At 125 °C the equilibrium is reached after 10 min, but at room temperature this is only obtained after a year or more. At each temperature the relaxation extends over 2–4 orders of magnitude in time and is much more gradual than a simple exponential. The decay is accurately described by a stretched exponential form,[29]

$$\Delta n_{BT} = \Delta n_0 \exp[-(t/\tau)^{\beta}] , \tag{15}$$

where Δn_{BT} is the departure of n_{BT} from its equilibrium value. The dispersion parameter β increases from 0.45 at room temperature to 0.7 at 125 °C. In another paper,[29] the stretched exponential and the temperature dependence of β are explained quantitatively by relating these to the measured dispersive time dependence of the hydrogen diffusion.

In Fig. 15 the temperature dependence of the relaxation time τ_E is shown. The solid points are taken from Fig. 1 in which the relaxation data is fitted to the stretched exponential form of Eq. (15). The other data are estimated from the dependence of n_{BT} on the cooling rates at different temperatures.[1] The fact that a quench rate of 2–5 °C/sec results in no further increase in n_{BT} above 220 °C, as in Fig. 6 of Ref. 1, implies that the sample has completely relaxed in the time to cool through this temperature, so that the relaxation time can be estimated, albeit imprecisely. These estimates are consistent with the direct measurements and show that the relaxation times are activated with an energy of about 0.95 eV and a prefactor of about 10^{-10} sec^{-1}. These data supercede the previous results which indicated that the activation energy decreased at low temperature, and

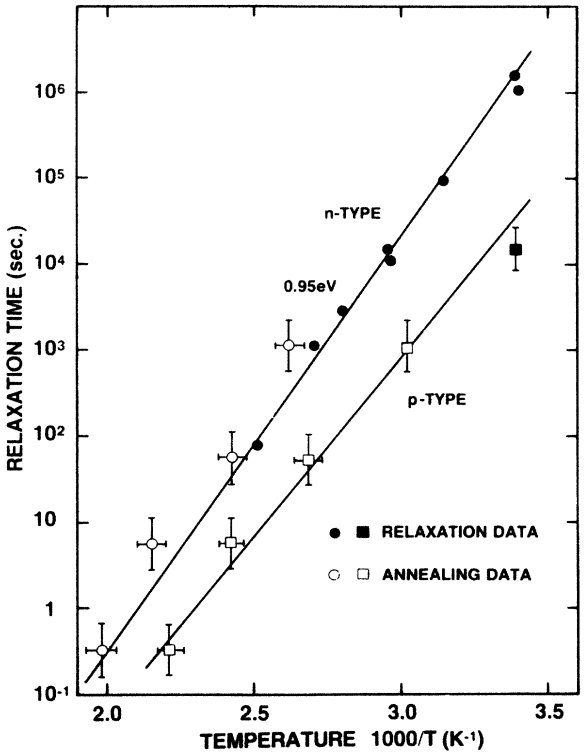

FIG. 15. The temperature dependence of the relaxation time obtained from relaxation and annealing data for n-type ($10^{-2}[PH_3]/[SiH_4]$) and p-type ($3\times10^{-3}[B_2H_6]/[SiH_4]$) films.

which were based on incomplete relaxation data. Results for p-type a-Si:H taken from Ref. 1 are also shown in Fig. 15. Complete relaxation curves have not yet been measured, so that these data are still rather approximate, but show that τ_E is again activated with relaxation times about an order of magnitude shorter than for n-type samples.

Both the activation energy and difference between p-type and n-type doping are consistent with the known hydrogen diffusion.[12] Although the diffusion data find a slightly higher activation energy of 1.2–1.3 eV, we have noted before that the time dependence of the diffusion leads to a slight overestimate of the energy.[12]

Further evidence for the role of hydrogen is given in Fig. 16 which shows 65 °C relaxation data for different doping levels from 10^{-2} to $10^{-5}[PH_3]/[SiH_4]$. Previously we reported that the decay was similar for all n-type samples.[1] The present more-detailed data show that there is a trend towards a longer relaxation time at lower doping levels. Since the hydrogen diffusion coefficient also decreases at lower doping levels, the results are further support for the role of hydrogen in the relaxation process.[30] The shape of the decay is a stretched exponential with about the same exponent for all doping levels.

Another feature of the relaxation is its dependence on the electronic state of the material. Figure 17(a) shows how the relaxation of n_{BT} at one particular temperature (65 °C) depends on the initial quenching conditions which give different frozen-in values of n_{BT}. Data are shown for quenching from 150, 210, and 250 °C, the last of these being quenched in water rather than air. The highest initial n_{BT} results in a faster decay with a time constant increased by a factor 2 compared to the lowest n_{BT}. However, when the change in n_{BT} from its equilibrium value is sufficiently small, the relaxation curves are almost indistinguishable, indicating that for small departures from

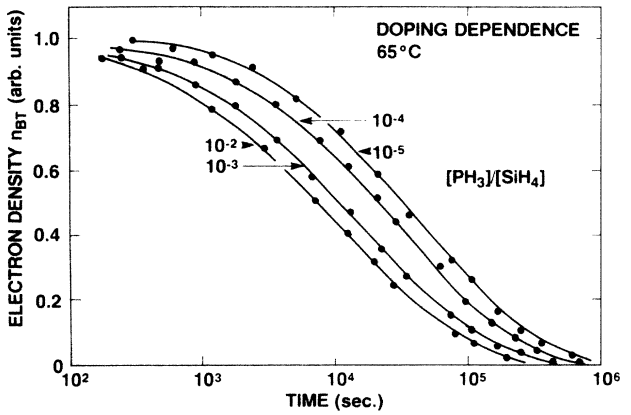

FIG. 16. The doping dependence of the relaxation of n_{BT} measured at 65 °C.

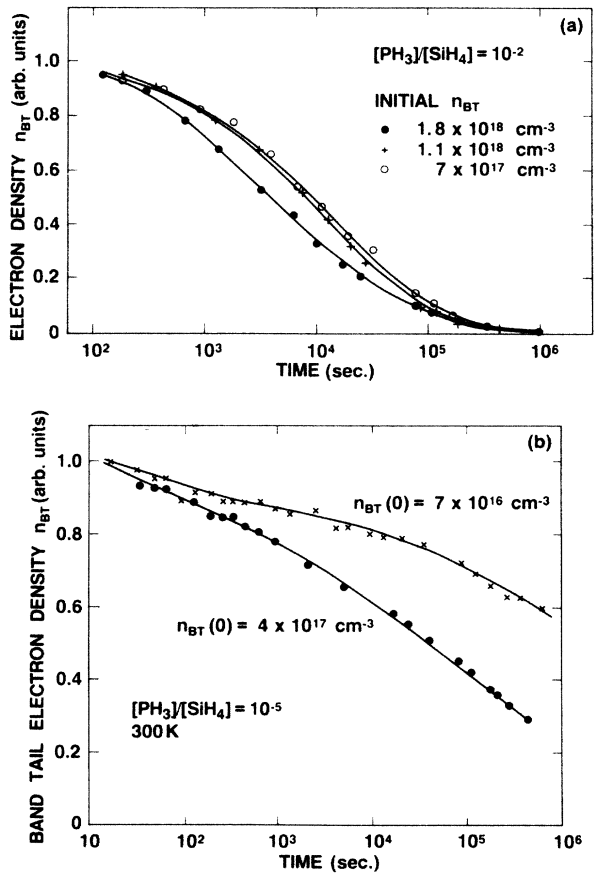

FIG. 17. (a) The normalized relaxation of n_{BT} in a heavily doped n-type sample at 65 °C, showing that the decay time decreases as the initial value of n_{BT} is increased by quenching from higher temperatures. (b) The normalized relaxation of n_{BT} in a lightly doped n-type sample at room temperature, showing that the decay time decreases and the shape of the decay changes as the initial value of n_{BT} is increased by bias annealing.

equilibrium a unique relaxation curve is obtained. Even for the larger initial n_{BT}, the shape of the decay is not significantly altered; it is simply shifted to shorter times. This result is important for the analysis of the stretched exponential relaxation which assumes that the decay is in the regime of a small deviation from equilibrium.

As the deviation from equilibrium gets larger, the form of the relaxation does change substantially. The bias-annealing results of Fig. 3 show that very large enhancements of n_{BT} can be obtained, and the room-temperature relaxation under these conditions is shown in Fig. 17(b). For the largest n_{BT}, a 30% reduction occurs within the first few minutes, whereas for smaller quenched in values of n_{BT} more than 10 times longer is required to observe the same relative change. Quenching without bias results in an even smaller initial n_{BT} and the decay is even slower.[1]

Evidently the relaxation rate is enhanced by the increased density of electrons, or by the shift of the Fermi energy, and this must be explained by any model of the relaxation. In fact, we argue that the increased relaxation rate for samples with a large quenched in n_{BT} is an inevitable consequence of the electronic equilibrium. To see this we note that the rate of change of N_{donor} or N_{DB} must be given by an expression of the form

$$dN_{donor}/dt = N_p r_c - N_{donor} r_{an} , \tag{16}$$

where r_c and r_{an} are the probabilities of creating and annihilating donors, with a similar expression applying to dangling bonds. Equilibrium occurs when $dN_{donor}/dt = 0$. We know that the equilibrium value of N_{donor} is related to n_{BT} at each temperature, otherwise we could not freeze in a nonequilibrium state, nor could we change the equilibrium in the bias-annealing experiments of Fig. 3. Consequently, one or both of r_c and r_{an} are functions of n_{BT}, so that dN_{donor}/dt certainly is also.

Thus it is no surprise that the relaxation rate increases with the excess n_{BT} and any model to explain the relaxation must include this dependence. The hydrogen diffusion model is again consistent with the results since D_H also depends on n_{BT}, as is seen from the doping dependence of the diffusion. The interpretation of the doping dependence is that the hydrogen release energy is decreased by an electron dropping from the Fermi energy to the dangling-bond state formed as the hydrogen is released. The model predicts that a larger n_{BT}, which raises E_F, will increase the diffusion. Thus although we have no data, we anticipate that, for example, illumination will increase D_H and a depletion bias will reduce it.

From all the above results we conclude that there is very strong evidence that hydrogen motion drives the structural changes that lead to thermal equilibrium (see Ref. 11 for further discussion).

VI. DISCUSSION

We now attempt to bring together the model for the electronic equilibrium with the underlying bonding changes. Our structural model is that the motion of hydrogen is the means by which the electronic equilibrium occurs. A complete explanation of the equilibrium must therefore relate hydrogen motion to the creation and annihilation of defects and donors, and this is now attempted.

A. The role of hydrogen in the electronic equilibrium

It has been pointed out before that hydrogen motion can easily change the coordination of both silicon and phosphorus by the release of hydrogen from Si—H or P—H bonds and by breaking Si—Si or Si—P bonds.[1,12,27,28,31] In fact, a key feature of the interpretation of hydrogen diffusion is that interstitial hydrogen does break weak Si—Si bonds,[12] and experimental evidence for this is that the hydrogen concentration increases when a-Si:H films are exposed to a hydrogen plasma.[11] Energy estimates also find that the required bond strain is reasonable.[12] The reaction of hydrogen with the silicon network is therefore described by the model depicted in Fig. 18(a). This assumes a distribution of Si—Si bond energies broadened by the network disorder. The vertical scale is the energy of the hydrogen atom in the Si—Si, so that the lowest energy corresponds to the weakest and most easily broken bond. Since it is known that hydrogen can move freely in and out of the growing film, the hydrogenation must be at or close to equilibrium, and so can be described by a chemical potential μ_H. If μ_H lies above some Si—Si bond energies, then these will be occupied, and thus changed into Si—H bonds.

A more realistic model of growth must take into account that the formation of Si—H bonds at the growing surface will cause a major rearrangement of the structure, and so will change the distribution of Si—Si bonds. We argue that the weak bonds that otherwise would lie near the chemical potential will be eliminated by the hydrogen, and that the resulting Si—H bonds will be so relaxed that they cannot easily revert to weak bonds. Thus the distribution of bond energies might be as in Fig. 18(b), with a minimum density near the chemical potential

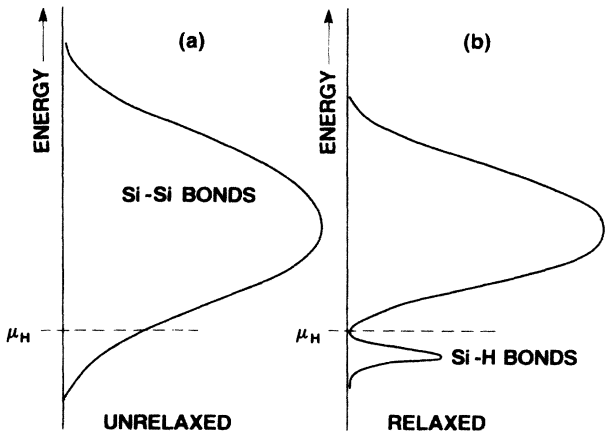

FIG. 18. A schematic diagram of the influence of hydrogen on the distribution of Si—Si and Si—H bonds in a-Si:H. (a) shows the chemical potential intersecting a hypothetical distribution of bonds. (b) shows the expected result when relaxation of the bonds during growth is included.

separating Si—H bonds from Si—Si bonds. The specific distribution will depend very much on the deposition conditions. We also expect that the distribution of Si—H bond energies will be relatively sharp, because they are largely decoupled from the distortions of the silicon network, but that the Si—Si distribution will be quite broad.

One way of understanding the distribution of Fig. 18(b) is to note that once a weak bond is broken by one hydrogen atom it will be energetically favorable for a second hydrogen to attach to the remaining dangling bond. If we denote the occupancy of a weak bond by zero, one, or two hydrogen atoms as W_0, W_1, and W_2, then the reaction

$$2W_1 \leftrightarrows W_0 + W_2 \tag{17}$$

is exothermic. This model of hydrogen in weak Si—Si bonds is therefore analogous to that of a negative-U defect, in that hydrogen has a tendency to pair on these sites. A negative U implies strong lattice relaxation which will necessarily occur at strained bonds.[12] In a negative-U model the chemical potential lies between the lower doubly occupied state and the higher empty state. This effect is then origin of μ_H lying in the minimum in the distribution shown in Fig. 18(b). For a simple negative-U model the density of singly occupied states is $N_0\exp(-E/2kT)$, where N_0 is the total density of states, and E is the energy difference between empty and doubly occupied states. However, it is clear that our description implies a broad distribution of N_0 and E.

One consequence of this model for hydrogen incorporation during growth is that as the chemical potential of the hydrogen is raised, the disorder of the silicon network will be reduced because the low-energy weak bonds are eliminated. The chemical potential increases with the concentration of atomic hydrogen in the plasma, so that the growth of microcrystalline films with a high hydrogen gas concentration is consistent with these ideas. In general, we expect a fundamental difference between the effects of atomic hydrogen during growth or subsequent to growth.

The motion of the hydrogen is included in the model illustrated in Fig. 19. Diffusion experiments conclude that hydrogen moves through in interstitial site about 1.5 eV above the Si-H energy, so that this interstitial band has been added to the distribution of Fig. 18(b). The diffusion is a process of excitation up to the interstitial level followed by trapping either at the weak bonds or at unoccupied Si-H sites, which are of course dangling bonds. In general, we expect there will be many more weak bond sites at which the hydrogen can be trapped than dangling bonds. On the other hand, most of the weak bond energies are very shallow and at these sites the trapping time is very short. This model seems able to account for the dispersive motion of hydrogen in just the same way as for electrons or holes in a band tail. After a hydrogen is excited to the interstitial level, it will be repeatedly trapped and released, but with increasing time it will sample deeper and deeper traps, thus reducing the diffusion coefficient. By analogy with models of dispersive electronic transport, an exponential distribution of weak bond energies will give a power-law time dependence for the hydrogen diffusion with a temperature dependence T/T_c as is observed.[32] This model is also similar to that used by Dyre, who describes a glass in terms of an exponentially decreasing density of configurations, with transitions from one state to another occurring by excitation to a higher-energy liquidlike state.[33] The time dependence of the system is then treated analogously to dispersive transport. Thus our description of Si—H bonding may also form a natural basis for the hydrogen-glass model of a-Si:H.[1]

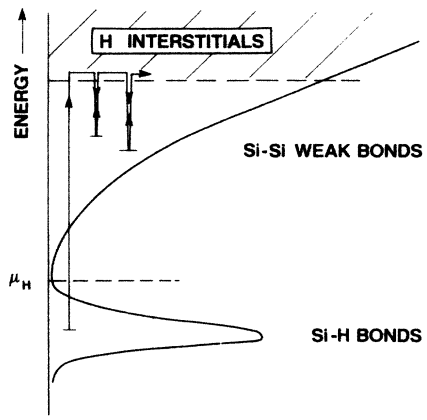

FIG. 19. A schematic diagram illustrating the Si—H bonds, the weak Si—Si bonds that can be broken by hydrogen, and the energy of the mobile hydrogen interstitials. A possible path for hydrogen diffusion is illustrated.

B. Discussion of the free-energy model

It must be emphasized that the free energy minimization model for the electronic equilibrium makes many simplifying assumptions, the most obvious being single values for the formation energies. The above description of hydrogen bonding makes it clear that the energies are expected to have a fairly broad distribution. This distribution may itself change as the hydrogen moves about. Furthermore, if dangling bonds can result when a weak bond is broken by hydrogen, or when hydrogen is released from an Si—H bond, then the defects may have two characteristically different local environments.

The different local bonding environments of Si and P atoms created during growth must also be considered. An assumption of the equilibrium model is that almost all phosphorus atoms were available to form donors, but only a small fraction of the silicon could form dangling bonds. There is a basic asymmetry in the conversion of threefold and fourfold states which may justify this assumption. Any threefold site can be made fourfold by the addition of hydrogen, which we expect is small enough not to be topologically hindered. On the other hand, the reverse process of removing a hydrogen atom will not apply to a fourfold site that is bonded only to other Si or P atoms. These can only be made threefold by breaking a bond. In equilibrium most of the silicon is fourfold and most phosphorus is threefold, so that donors can be created at any P atom but dangling bonds only at a subset of Si atoms. The real bonding structure is there-

fore very complex.

In addition to the effects of the particular bonding structures, any dependence of the formation energies on the electronic energy level of the donor or dangling bond has also been neglected. Also, no effects of the Coulomb interaction between the charged states have been included, which might result in a doping dependence of the shape of the density of states, the formation energies, and even the position of the mobility edge.

Despite the many approximations, the model described is very successful in its ability to reproduce the electronic properties of *a*-Si:H, starting only from minimizing the free energy. Clearly, a more realistic model for the distribution of formation energies is needed. Hopefully, the introduction of such a distribution would remove the remaining differences between model and experiment, but in the absence of a clear understanding of the distribution, we have not made further calculations.

The one observation that is the most puzzling is the lack of temperature dependence of the dangling-bond density in the equilibrium state. The cancellation of the energies in Eq. (11) would be a surprising coincidence. It seems to us that a similar puzzle also applies to the equilibrium in undoped *a*-Si:H. The experimental information to date indicates that the dangling-bond density changes by a factor of about 2 over the investigated range of freezing temperatures.[3,4] The change in N_{DB} can be easily predicted from an assumption that both N_{DB} and the time to reach equilibrium are activated,

$$N_{DB}=N_0\exp(-E_d/kT)\ , \tag{18}$$

$$\tau=\tau_0\exp(E/kT)\ . \tag{19}$$

From these equations one obtains

$$N_{DB}/N_0=(\tau/\tau_0)^{E_0/E}\ . \tag{20}$$

In annealing and cooling experiments, the highest and lowest temperatures at which the equilibrium can be monitored corresponds to fast quenching with a time constant of, say ~ 0.1 sec, and a long anneal, say for one day, with $t\sim 10^5$ sec. Thus the expected range of N_{DB} is $10^{6Ed/E}$. E_d is estimated to be 0.5–0.6 eV,[10] and E cannot be larger than 1.5 eV to give equilibrium in the observable temperature range. Therefore the expected observable range of N_{DB} is about 100 To explain the smaller observed variation requires $E_d\sim 0.1$ eV, which is apparently inconsistent with the measured density. Evidently, there is still much more to be understood in the equilibration process.

VII. SUMMARY

The main points of the paper are as follows.

(1) In equilibrium, the band-tail charge n_{BT} is activated with an energy 0.15–0.25 eV. The equilibration of n_{BT} is dominated by changes in the density of donors rather than by dangling bonds which are almost independent of temperature. These results are the first clear evidence that the donors equilibrate.

(2) The equilibrium can be modeled successfully using a free-energy minimization approach, assuming electronic equilibration of the donor and dangling-bond states, but not of the distribution of the band tails. The modeling gives excellent consistency between the measurements of n_{BT} and the conductivity, and despite several simplifying assumptions, we show that the full electronic properties can be well reproduced directly from the free-energy minimization.

(3) The relaxation of n_{BT} towards equilibrium follows a stretched exponential time dependence. The time constant is activated with an energy of about 1 eV, but the time constant also depends on the initial value of n_{BT} and on the doping level. These results provide further evidence that the motion of hydrogen causes the equilibration of the electronic states. An important process is believed to be creation of dangling bonds by hydrogen-breaking weak bonds.

(4) The model has difficulty in accounting for the temperature independence of the dangling-bond density which requires a better understanding of the equilibration reactions at an atomic level, and of the distribution of formation energies.

ACKNOWLEDGMENTS

We are grateful to C. C. Tsai for providing samples and to J. Kakalios for many helpful discussions. This research is supported by the Solar Energy Research Institute (Golden, CO).

[1]R. A. Street, J. Kakalios, C. C. Tsai, and T. M. Hayes, Phys. Rev. B **35**, 1316 (1987).
[2]R. A. Street, J. Kakalios, and T. M. Hayes, Phys. Rev. B **34**, 3030 (1986).
[3]Z. Smith, S. Aljishi, D. Slobodin, V. Chu, S. Wagner, P. M. Lenahan, R. R. Arya, and M. S. Bennett, Phys. Rev. Lett. **57**, 2450 (1986).
[4]T. J. McMahon and R. Tsu, Appl. Phys. Lett. **51**, 412 (1987).
[5]J. Kakalios and R. A. Street, Phys. Rev. B **34**, 6014 (1986).
[6]Z. Smith and S. Wagner, Phys. Rev. B **32**, 5510 (1985).
[7]G. Muller, S. Kalbitzer, and H. Mannsperger, Appl. Phys. A **39**, 243 (1986); H. Mansperger, S. Kalbitzer, and G. Muller, *ibid.* **41**, 253 (1986).
[8]Y. Bar-Yam, D. Adler, and J. D. Joannopoulos, Phys. Rev. Lett. **57**, 467 (1986).
[9]Z. Smith and S. Wagner, Phys. Rev. Lett. **59**, 688 (1987).
[10]R. A. Street, Phys. Rev. Lett. **49**, 1187 (1982).
[11]R. A. Street, Mater. Res. Soc. Symp. Proc. (to be published).
[12]R. A. Street, C. C. Tsai, W. B. Jackson, and J. Kakalios, Philos. Mag. B **56**, 305 (1987).
[13]R. A. Street and J. Zesch, Philos. Mag. B **50**, L19 (1984).
[14]M. Hack, R. A. Street, and M. Shur (unpublished).
[15]R. A. Street and J. Kakalios, Philos. Mag. B **54**, L21 (1986).
[16]D. V. Lang, J. D. Cohen, and J. P. Harbison, Phys. Rev. Lett. **48**, 421 (1982).
[17]G. A. Swartz, Appl. Phys. Lett. **44**, 697 (1984).
[18]W. B. Jackson, S. M. Kelso, C. C. Tsai, J. W. Allen, and S.-J. Oh, Phys. Rev. B **31**, 5187 (1985).

[19]J. M. Marshall, R. A. Street, and M. J. Thompson, Philos. Mag. B **54**, 51 (1986).
[20]W. E. Spear, J. Non-Cryst. Solids **59&60**, 1 (1983).
[21]N. M. Johnson, Appl. Phys. Lett. **42**, 981 (1983).
[22]D. V. Lang, J. D. Cohen, and J. P. Harbison, Phys. Rev. B **25**, 5285 (1982).
[23]R. A. Street, D. K. Biegelsen, and J. C. Knights, Phys. Rev. B **24**, 969 (1981).
[24]D. Monroe, Phys. Rev. Lett. **54**, 146 (1985).
[25]M. Stutzmann, D. K. Biegelsen, and R. A. Street, Phys. Rev. B **35**, 5666 (1987).
[26]R. A. Street and J. Kakalios, Phys. Rev. Lett. **58**, 2504 (1987).
[27]D. E. Carlson, Appl. Phys. A **41**, 305 (1986).
[28]M. Stutzmann, Philos. Mag. **56**, 63 (1987).
[29]J. Kakalios, R. A. Street, and W. B. Jackson, Phys. Rev. Lett. **59**, 1037 (1987).
[30]The measurements are performed with relatively low quenching temperatures, but the exact doping dependence may vary slightly on the details of the quenching, as shown in Fig. 17 and the discussion.
[31]W. B. Jackson, Solar Cells **21**, 431 (1987).
[32]T. Tiedje and A. Rose, Solid State Commun. **37**, 49 (1981).
[33]J. C. Dyre, Phys. Rev. Lett. **58**, 792 (1987).